NASA TECHNICAL NOTE

NASA TN D-3274

NASA TN D-3274
c.1
LOAN COPY: R
AFWL (W
KIRTLAND AFI
0079796
TECH LIBRARY KAFB, NM

EFFECTS OF MODEL GEOMETRIC ACCURACY ON COMPARISON OF WIND-TUNNEL AND FLIGHT PRESSURE MEASUREMENTS ON A LAUNCH VEHICLE

by Thomas C. Kelly, George C. Greene, and Robert J. Keynton

Langley Research Center
Langley Station, Hampton, Va.

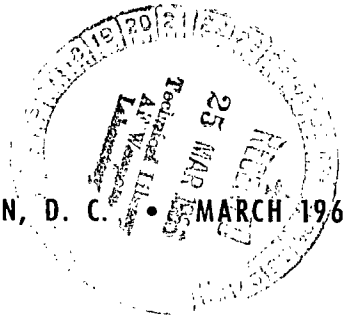

NATIONAL AERONAUTICS AND SPACE ADMINISTRATION • WASHINGTON, D. C. • MARCH 1966

TECH LIBRARY KAFB, NM
0079796

NASA TN D-3274

EFFECTS OF MODEL GEOMETRIC ACCURACY ON COMPARISON OF WIND-TUNNEL AND FLIGHT PRESSURE MEASUREMENTS ON A LAUNCH VEHICLE

By Thomas C. Kelly, George C. Greene,
and Robert J. Keynton

Langley Research Center
Langley Station, Hampton, Va.

NATIONAL AERONAUTICS AND SPACE ADMINISTRATION

For sale by the Clearinghouse for Federal Scientific and Technical Information
Springfield, Virginia 22151 – Price $2.00

EFFECTS OF MODEL GEOMETRIC ACCURACY ON COMPARISON OF WIND-TUNNEL AND FLIGHT PRESSURE MEASUREMENTS ON A LAUNCH VEHICLE

By Thomas C. Kelly, George C. Greene,
and Robert J. Keynton
Langley Research Center

SUMMARY

Full-scale flight and model-scale wind-tunnel investigations have been conducted to determine the variation with Mach number of pressures on a rearward-facing transition flare on the RAM B launch vehicle and effects of model accuracy on comparisons of the wind-tunnel and flight results. Flight results were obtained at Mach numbers from about 0.20 to 4.00 and wind-tunnel results were measured over a Mach number range from 0.20 to 1.20 at an angle of attack of 0°.

The full-scale flight measurements indicated that a remarkably abrupt and severe pressure drop (3 psi (20.684 kN/m^2) in 0.1 second) occurred between Mach numbers of 0.90 and 0.95 on the rear-facing flare. Based upon the wind-tunnel investigations, this pressure drop was associated with the attachment on the flare of a separated flow.

Agreement was generally good when the results for the modified model (where a small rear-facing step was located just upstream of the rearward-facing flare) were compared with those for the full-scale vehicle. Both the Mach number at which the pressure drop occurred in flight and the magnitude of the change in pressure coefficient agreed particularly well with the wind-tunnel results. Comparison of the wind-tunnel results of the original model (where the small rear-facing step was not duplicated) with the results obtained during the flight investigation gave relatively poor agreement at subsonic speeds.

INTRODUCTION

The Langley Research Center of the National Aeronautics and Space Administration has been conducting a series of rocket flight experiments to investigate the phenomena associated with communications blackout during reentry. The launch vehicle employed in the investigations is designated the RAM B (Radio Attenuation Measurement) and is a three-stage, solid-propellant, unguided vehicle. A detailed description of the vehicle and its flight

performance may be obtained in reference 1. Wind-tunnel investigations of the RAM B reported in reference 2 indicated that as a result of a separated flow reattachment, abrupt and sizable pressure variations occurred at high subsonic speeds over a rear-facing frustum located downstream of the third-stage separation plane. Based upon the wind-tunnel results and predicted flight trajectories, it was estimated that a pressure decrease of about 3 psi (20.684 kN/m^2) could occur over most of the rear-facing frustum as Mach number was increased from 0.90 to 0.95 and that the decrease would occur in 1/2 second or less (see ref. 2). These results indicated a potential vehicle venting problem; namely, that vent orifices were located on the rear-facing frustum in order to reduce pressure differentials across the vehicle structure in this region and that an extremely abrupt pressure drop could reduce the vent effectiveness. In view of these indications, the preliminary venting arrangement for the RAM vehicles was redesigned and the attachment of the rear-facing frustum was significantly strengthened. In addition, the RAM B3 flight vehicle (the only flight vehicle on which pressure measurements on the rear-facing flare were feasible) was instrumented in an effort to determine whether pressure variations similar to those noted in the wind-tunnel investigation also occurred at the much higher Reynolds numbers associated with full-scale flight. The RAM B3 flight test was conducted from the NASA Wallops Station on April 10, 1964, and the venting arrangement performed satisfactorily.

Preliminary comparisons of the flight and wind-tunnel pressure measurements indicated poor agreement at subsonic speeds; furthermore, the results suggested the presence of separated flow over the rear-facing frustum for the full-scale flight case and attached flow for the model investigation at the lower subsonic Mach numbers. As a result, additional wind-tunnel investigations were conducted employing a model on which a small rear-facing step was duplicated. This step was located just upstream of the rear-facing frustum on the full-scale vehicle.

The present paper contains comparisons of the flight and wind-tunnel results at Mach numbers from about 0.20 to 1.20 showing the effects of duplicating the rear-facing step. Included are flight pressure data obtained over a Mach number range from about 0.20 to 4.00. Reynolds numbers, based on first-stage diameter, ranged from about 0.2×10^6 to 27.6×10^6 for the flight data and from 0.2×10^6 to 1.3×10^6 for the wind-tunnel results. Because of tunnel equipment limitations, flight Reynolds numbers could not be simulated during the wind-tunnel investigation except at a Mach number of 0.20.

SYMBOLS

Measurements for this investigation were taken in the U.S. Customary System of Units. Equivalent values are indicated herein parenthetically in the International System (SI) in the interest of promoting use of this system in future NASA reports. Details concerning the use of SI, together with physical constants and conversion factors, are given in reference 3.

C_p pressure coefficient, $\frac{p_l - p}{q}$

l	overall length, measured from theoretical nose-cone apex to fin trailing edge; model-scale 51.39 in. (130.5 cm), full-scale 510.31 in. (1296.1 cm)
M	Mach number
p	tunnel or flight free-stream static pressure
p_l	local static pressure
$p_{t,\infty}$	tunnel stagnation pressure
q	free-stream dynamic pressure
R	Reynolds number based on first-stage diameter
x	longitudinal distance, measured from theoretical nose-cone apex
α	angle of attack of body center line
ϕ	orifice-row orientation angle, measured clockwise from vertical as viewed from front

APPARATUS, TESTS, AND PROCEDURE

Flight Investigation

A general description of the RAM B2 vehicle including selected details of the mechanical design, fabrication, and flight performance is given in reference 1. The present flight vehicle, designated RAM B3, has some minor dimensional differences in the region of the third-stage separation plane from the vehicle of reference 1 (RAM B2); these differences may be noted by a comparison of figure 1 of the present paper with figure 5 of reference 1.

For the flight investigation, the local pressure (at $x/l = 0.327$) on the reverse flare (fig. 1) was measured by using a 15 psia (103.42 kN/m^2) pressure transducer. The transducer is designed to operate between temperature limits of -65° F and 200° F (219.3° K and 366.5° K) and has a response capability of measuring 63 percent of a step pressure change in 20 milliseconds or less. Estimated accuracy for the gage is ±0.15 psia (±1.03 kN/m^2). The pressure was measured at only one location on the reverse flare because only a single telemeter channel was available for this phase of the flight investigation. In view of the abrupt nature of the pressure variations noted in the wind-tunnel tests, the local pressure at $x/l = 0.327$ was measured continuously from launch to second-stage ignition. Examination of the flight results showed the vehicle angle of attack to be approximately 0° throughout the period during which pressures were recorded. Furthermore, it would be expected that because the vehicle is spin stabilized, any effects on flare pressures of small variations in angle of attack would be effectively reduced. The flight results are given in

table I. Selected photographs of the RAM vehicle and the reverse-flare region are presented in figure 2.

Wind-Tunnel Investigation

The model used for the present wind-tunnel investigation was obtained by modifying the model of reference 2 in the region of the third-stage-separation plane in order to duplicate a small rear-facing step which occurred at the juncture of the flare—reverse-flare transition section on the flight vehicle. (See figs. 1 and 2(b).) Additional pressure orifices were also installed to provide an improved coverage over the region of the flare at which the orifice was installed on the full-scale configuration. Photographs of the wind-tunnel model are presented in figure 3.

The investigation was conducted in the Langley 8-foot transonic pressure tunnel. This facility is a single-return, slotted-throat tunnel having controls which allow for the independent variation of Mach number, stagnation pressure, temperature, and humidity. The tunnel results were obtained at selected Mach numbers from 0.20 to 1.20 at an angle of attack of 0°. Boundary-layer transition was artificially fixed by using a transition strip on the model nose cone. Most of the results were obtained at Reynolds numbers corresponding to a tunnel stagnation pressure of approximately 2120 psf (101.51 kN/m^2); however, selected results were also obtained at a stagnation pressure of 1060 psf (50.75 kN/m^2). Wind-tunnel model pressures were measured with the use of liquid manometers which were photographically recorded. The wind-tunnel results are presented in table II in the form of pressure coefficients.

RESULTS AND DISCUSSION

A comparison of the Reynolds numbers for the wind-tunnel and flight investigations is presented in figure 4; the Reynolds numbers are based on the first-stage diameter. Full-scale Reynolds numbers were duplicated only at a Mach number of 0.20 during the wind-tunnel investigation. Figure 5(a) gives the variation with Mach number of the reverse-flare pressure coefficients determined from flight results, whereas figure 5(b) presents selected flight results of the local pressure as a function of time. A comparison of the longitudinal pressure distributions determined from wind-tunnel measurements on the original model (ref. 2) and the modified model (present tests) is shown in figure 6. The effects of tunnel stagnation pressure on pressure distributions for the modified model configuration are given in figure 7 for selected Mach numbers from 0.20 to 1.00. Figure 8 presents a comparison of the variations of pressure coefficient with Mach number for the two model configurations and the full-scale vehicle for the orifice location utilized in the full-scale flight investigation.

Flight Results

The pressures measured on the rearward-facing flare during flight are presented in figure 5(a) in terms of the variation of pressure coefficient with

Mach number. Significant Mach number effects are noted, the most outstanding being the sudden pressure drop (increase in the value of negative C_p) which occurs between Mach numbers of 0.90 and 0.95. It was in this Mach number range that a similar abrupt pressure drop, which was found to be associated with a separated flow reattachment on the reverse flare, occurred in the wind-tunnel tests of the original model. A plot of this portion of the curve, wherein the actual measured local pressure is presented as a function of time (fig. 5(b)), shows the extremely abrupt nature of the pressure drop, with a change in pressure of about 3 psi (20.684 kN/m^2) occurring in about 0.1 second. Immediately after the drop, a rapid increase in pressure coefficient with increasing Mach number is noted and this increase continues (at a gradually diminishing rate) up to a Mach number of 4.00 (fig. 5(a)). These flight results, which show the reverse-flare pressure variations to be even more abrupt than anticipated from the wind-tunnel investigations, illustrate the significant problems associated with the design of vent systems for regions on launch vehicles where similar flow variations would be encountered – for example, just downstream of a relatively high angle nose-cone-cylinder juncture where flow separation would probably be present at subsonic speeds. The problem is further complicated by the lack of theoretical methods which might be used to predict pressure distributions accurately in the transonic mixed-flow region or, more importantly, to predict the rate of pressure change at a given location resulting from small Mach number changes since these variations are generally required for the vent design. As a matter of interest, the RAM flight measurements indicated that pressure reductions occurred at a rate of about 70 psi (492.63 kN/m^2) per second during the abrupt pressure drop near a Mach number of 0.95.

Wind-Tunnel Results

A comparison of the longitudinal pressure distributions for the original and modified model configurations, given in figure 6, shows that sizable effects are noted when the small step upstream of the rear-facing frustum is simulated. For the original-model investigation reported in reference 2, the step was not duplicated; in fact, the juncture was slightly rounded. (See fig. 2(b) of ref. 2.) Figure 6 shows that the presence of the rear-facing step on the modified model causes flow separation to occur at noticeably lower Mach numbers ($M \approx 0.6$ for the modified model and $M \approx 0.7$ for the original model) and the severity of the separation is considerably greater for the modified model than for the original model. It is interesting to note also that, except for highly localized variations at the step location, the pressure distributions are very nearly identical at Mach numbers from 0.95 to 1.20 for both configurations.

Results showing the effect of tunnel stagnation pressure on pressure distributions for the modified model are given in figure 7. The results show negligible effects of stagnation pressure or, therefore, Reynolds number at a Mach number of 0.20 where the flow is apparently attached. At intermediate Mach numbers ($M = 0.40$ to 0.80), increasing Reynolds number results in a slight decrease in the apparent severity of flow separation, and at the highest Mach number ($M = 1.00$), little effect of Reynolds number is again noted. It should be noted that the Reynolds number effect noted at intermediate Mach numbers,

although small, is considered to be valid, based upon estimated pressure-coefficient accuracies to be expected at these Mach numbers.

Comparison of Results

In figure 8, the variations of local pressure coefficient with Mach number are given for the original and modified model configurations and are for an orifice location that corresponds to the location used in the full-scale flight investigation $\left(\frac{x}{l} = 0.327\right)$. Results from the flight investigation are included for comparison. Comparison of the original-model and modified-model results indicates that significant differences occur at Mach numbers below 0.95. These differences are a result of the aforementioned variations in the occurrence and severity of flow separation between the two model configurations. At the higher Mach numbers (0.95 to 1.20), the modified-model results are in excellent agreement with those for the original model.

Comparison of the original-model results with the full-scale flight-vehicle results shows that at subsonic speeds, the agreement is poor. Comparison of the results for the modified model and flight vehicle, however, indicates excellent agreement at Mach numbers from 0.60 to 0.90 and fair agreement at the lower Mach numbers. In addition, both the Mach number at which the pressure drop occurs in flight and the magnitude of the pressure drop are in good agreement with the modified model results. At the lower Mach numbers, however, the pressure coefficients are subject to relatively large errors resulting from the reduced values of dynamic pressure. For example, at a Mach number of 0.20, the dynamic pressure for both the flight and tunnel investigations is of the order of 60 psf (2.87 kN/m^2). This low dynamic pressure, coupled with a consideration of the accuracy of the local-pressure measurement, indicates that pressure coefficients at a Mach number of 0.20 can be in error by as much as ± 0.36 and ± 0.05 for the flight and tunnel investigations, respectively. It should also be noted that possible effects of Reynolds number may not be discounted at Mach numbers higher than 0.20.

At the higher Mach numbers (M = 0.95 to 1.20), comparison of the tunnel and flight results indicates the existence of a constant shift in pressure-coefficient level between the flight and wind-tunnel investigations; however, the variations with Mach number are essentially identical. Although the reason for the shift is not known, it is conjectured that for these speeds where the flow is attached (M = 0.95 to 1.20), small differences between the flight and model configurations which were not simulated during the wind-tunnel investigation (for example, frustum angles and lengths) have a strong effect. At lower Mach numbers, because of the separated flow condition, it would be expected that small configuration differences would have only slight effects on the rear-facing frustum pressures. However, effects of Reynolds number may also be a contributing factor.

Although only limited results were available for the flight and wind-tunnel comparisons, these results do indicate the need for close attention to vehicle geometric details. In particular, for regions of scaled models which may be

critical with regard to flow separation (for example, when an abrupt surface discontinuity occurs within an adverse pressure gradient), an accurate simulation of detailed geometry is required.

CONCLUDING REMARKS

Flight and wind-tunnel investigations, conducted to determine the variation with Mach number of pressures on a rearward-facing transition flare on the RAM B launch vehicle and the effects of duplicating a small rear-facing step located at the upstream end of the flare, have indicated the following results:

1. The full-scale flight measurements indicated that a remarkably abrupt and severe pressure drop occurred between Mach numbers of 0.90 and 0.95 on the rear-facing flare. Based upon the wind-tunnel investigations, this pressure drop (3 psi (20.684 kN/m^2) in 0.1 second) was associated with the attachment on the flare of a separated flow.

2. Agreement was generally good when the results for the modified model (where a small rear-facing step was located just upstream of the rearward-facing flare) were compared with those for the full-scale vehicle. Both the Mach number at which the pressure drop occurred in flight and the magnitude of the change in pressure coefficient agreed particularly well with the wind-tunnel results.

3. Comparison of the wind-tunnel results of the original model (where the small rear-facing step was not duplicated) with the results obtained during the flight investigation gave relatively poor agreement at subsonic speeds.

Langley Research Center,
National Aeronautics and Space Administration,
Langley Station, Hampton, Va., November 8, 1965.

REFERENCES

1. Raper, James L.; Keynton, Robert J.; and Woodbury, Gerald E.: Detailed Description and Flight Performance of the RAM B Vehicle. NASA TN D-2437, 1964.

2. Kelly, Thomas C.; and Keynton, Robert J.: Longitudinal Aerodynamic Characteristics and Surface Pressure Measurements for a 1/10-Scale Model of the RAM B Launch Vehicle. NASA TN D-2204, 1964.

3. Mechtly, E. A.: The International System of Units - Physical Constants and Conversion Factors. NASA SP-7012, 1964.

TABLE I.- RAM B3 FLIGHT RESULTS

Time, sec	Mach number	Dynamic pressure		Ambient pressure		Reverse-flare pressure		Altitude		Velocity	
		psf	kN/m^2	psia	kN/m^2	psia	kN/m^2	ft	m	ft/sec	m/sec
0.50	0.051	3.87	0.19	14.69	0.70	14.70	0.70	12.0	3.7	57.11	17.41
1.00	.102	15.43	.74	14.67	.70	14.65	.70	47.3	14.4	114.04	34.76
1.50	.153	34.49	1.65	14.64	.70	14.70	.70	107.8	32.9	170.61	52.00
2.00	.203	60.77	2.91	14.60	.70	14.52	.70	191.0	58.2	226.76	69.12
2.50	.253	93.83	4.49	14.54	.70	14.40	.69	297.8	90.8	282.22	86.02
3.05	.307	137.54	6.59	14.46	.70	14.22	.68	442.0	134.7	342.40	104.37
3.55	.356	184.20	8.82	14.38	.69	13.90	.67	595.7	181.6	397.14	121.05
4.05	.406	237.49	11.37	14.29	.68	13.66	.65	770.5	234.8	452.10	137.80
4.55	.456	297.30	14.23	14.19	.68	13.38	.64	963.7	293.7	507.28	154.62
5.05	.506	363.68	17.41	14.08	.67	13.11	.63	1177.5	358.9	562.84	171.55
5.55	.557	436.83	20.92	13.96	.67	12.69	.61	1410.3	429.9	618.97	188.66
6.05	.609	516.60	24.74	13.84	.66	12.31	.59	1661.0	506.3	675.62	205.93
6.55	.661	603.04	28.87	13.70	.66	11.89	.57	1931.0	588.6	732.88	223.38
7.05	.714	696.13	33.33	13.56	.65	11.48	.55	2220.0	676.7	790.81	241.04
7.55	.767	795.66	38.10	13.40	.64	10.87	.52	2526.5	770.1	849.31	258.87
8.05	.821	900.87	43.13	13.24	.63	10.38	.50	2851.8	869.2	908.11	276.79
8.55	.876	1011.07	48.41	13.08	.63	9.71	.46	3195.8	974.1	967.01	294.74
9.05	.930	1125.36	53.88	12.90	.62	8.61	.41	3556.8	1084.1	1025.73	312.64
9.55	.984	1241.22	59.43	12.72	.61	4.96	.24	3935.5	1199.5	1083.38	330.21
10.05	1.036	1357.19	64.98	12.54	.60	5.09	.24	4329.7	1319.7	1139.60	347.35
10.55	1.089	1476.88	70.71	12.35	.59	5.16	.25	4740.8	1445.0	1196.20	364.60
11.05	1.143	1600.50	76.63	12.15	.58	5.28	.25	5166.5	1574.7	1253.30	382.01
11.55	1.198	1727.83	82.73	11.95	.57	5.31	.25	5609.5	1709.8	1311.00	399.59
12.05	1.253	1858.89	89.00	11.75	.56	5.33	.26	6066.8	1849.2	1369.30	417.36
15.05	1.603	2706.71	129.60	10.45	.50	4.79	.23	9142.0	2786.5	1732.60	528.10
18.05	1.991	3621.96	173.42	9.07	.43	3.94	.19	12780.0	3895.3	2122.90	647.06
21.05	2.424	4534.40	217.11	7.65	.37	3.20	.15	16988.8	5178.2	2543.70	775.32
25.05	3.122	5712.00	273.49	5.81	.28	2.44	.12	23553.8	7179.2	3191.40	972.74
30.05	4.016	6083.60	291.28	3.74	.18	1.41	.07	33379.8	10174.2	3936.40	1199.81

TABLE II.- SURFACE PRESSURE COEFFICIENTS FOR FLARE—REVERSE-FLARE TRANSITION SECTION OF MODIFIED MODEL CONFIGURATION

$[\phi = 0^\circ; \alpha = 0^\circ]$

(a) $p_{t,\infty}$ = 2120 psf (101.51 kN/m^2); M = 0.20 to 0.80

x/l	C_p for -						
	M = 0.20	M = 0.40	M = 0.60	M = 0.65	M = 0.70	M = 0.75	M = 0.80
0.258	0.265	0.296	0.340	0.348	0.357	0.371	0.377
.278	.080	.079	.128	.136	.143	.160	.175
.311	-.637	-.599	-.487	-.471	-.459	-.443	-.436
*.313	-.796	-.714	-.531	-.507	-.491	-.469	-.460
.314	-.743	-.671	-.531	-.510	-.491	-.475	-.468
.317	-.477	-.570	-.498	-.484	-.474	-.459	-.455
.320	-.265	-.447	-.469	-.465	-.462	-.453	-.453
.324	-.159	-.310	-.421	-.435	-.444	-.443	-.451
.325	-.133	-.296	-.414	-.432	-.442	-.440	-.448
.327	-.106	-.253	-.395	-.419	-.433	-.437	-.448
.328	-.053	-.195	-.366	-.396	-.418	-.429	-.443
.331	-.027	-.123	-.318	-.364	-.398	-.416	-.438
.335	.027	-.051	-.260	-.318	-.365	-.395	-.426
.338	.053	-.007	-.212	-.276	-.336	-.373	-.411
.342	.027	.022	-.110	-.179	-.251	-.309	-.367
.351	.027	.029	.029	-.010	-.070	-.139	-.227
.356	.000	.022	.055	.036	-.003	-.059	-.140
.374	.000	.000	.048	.055	.061	.067	.039
.394	.000	-.007	.022	.029	.038	.051	.059
.414	.000	-.007	.018	.019	.023	.032	.042
.433	.000	.007	.029	.032	.035	.040	.044
.453	.000	.022	.051	.049	.050	.056	.057

*Orifice located immediately downstream of step.

TABLE II.- SURFACE PRESSURE COEFFICIENTS FOR FLARE—REVERSE-FLARE TRANSITION SECTION OF MODIFIED MODEL CONFIGURATION - Continued

(b) $p_{t,\infty}$ = 2120 psf (101.51 kN/m^2); M = 0.85 to 1.20

x/l	C_p for -					
	M = 0.85	M = 0.90	M = 0.94	M = 0.95	M = 1.00	M = 1.20
0.258	0.395	0.423	0.440	0.450	0.471	0.397
.278	.197	.227	.254	.266	.340	.406
.311	-.411	-.356	-.302	-.282	-.188	.037
*.313	-.448	-.477	-1.234	-1.205	-1.067	-.682
.314	-.459	-.492	-.946	-.921	-.794	-.456
.317	-.452	-.481	-1.068	-1.039	-.907	-.555
.320	-.448	-.477	-1.023	-.994	-.862	-.526
.324	-.450	-.483	-.971	-.945	-.813	-.498
.325	-.448	-.479	-.963	-.935	-.807	-.493
.327	-.450	-.483	-.957	-.929	-.801	-.487
.328	-.450	-.483	-.930	-.904	-.778	-.473
.331	-.448	-.481	-.825	-.851	-.731	-.446
.335	-.443	-.479	-.541	-.565	-.463	-.270
.338	-.436	-.475	-.461	-.462	-.362	-.159
.342	-.411	-.455	-.353	-.381	-.293	-.120
.351	-.301	-.367	-.180	-.268	-.213	-.085
.356	-.227	-.306	-.107	-.205	-.184	-.070
.374	-.016	-.101	.033	-.023	-.111	-.045
.394	.060	.032	.062	.043	-.080	-.028
.414	.057	.067	.056	.059	-.061	-.016
.433	.055	.069	.058	.074	-.027	.002
.453	.064	.076	.076	.090	.039	.031

*Orifice located immediately downstream of step.

TABLE II.- SURFACE PRESSURE COEFFICIENTS FOR FLARE—REVERSE-FLARE TRANSITION SECTION OF MODIFIED MODEL CONFIGURATION - Concluded

(c) $p_{t,\infty}$ = 1060 psf (50.75 kN/m^2); M = 0.20 to 1.00

x/l	C_p for -				
	M = 0.20	M = 0.40	M = 0.60	M = 0.80	M = 1.00
0.258	0.319	0.317	0.329	0.369	0.465
.278	.106	.115	.124	.177	.336
.311	-.638	-.519	-.447	-.409	-.203
*.313	-.798	-.592	-.469	-.419	-.985
.314	-.798	-.592	-.476	-.433	-.837
.317	-.479	-.505	-.461	-.428	-.899
.320	-.213	-.404	-.432	-.419	-.853
.324	-.160	-.303	-.410	-.423	-.817
.325	-.106	-.289	-.403	-.419	-.806
.327	-.106	-.245	-.395	-.419	-.798
.328	-.053	-.202	-.381	-.419	-.778
.331	.000	-.144	-.351	-.414	-.727
.335	.053	-.072	-.315	-.409	-.461
.338	.053	-.029	-.278	-.399	-.344
.342	.053	.029	-.183	-.369	-.282
.351	.000	.058	-.015	-.246	-.211
.356	.000	.058	.037	-.167	-.184
.374	.000	-----	.051	.030	-.113
.394	.000	-----	.029	.064	-.086
.414	.000	-----	.015	.049	-.063
.433	.000	-----	.022	.044	-.035
.453	.000	-----	.044	.059	.031

*Orifice located immediately downstream of step.

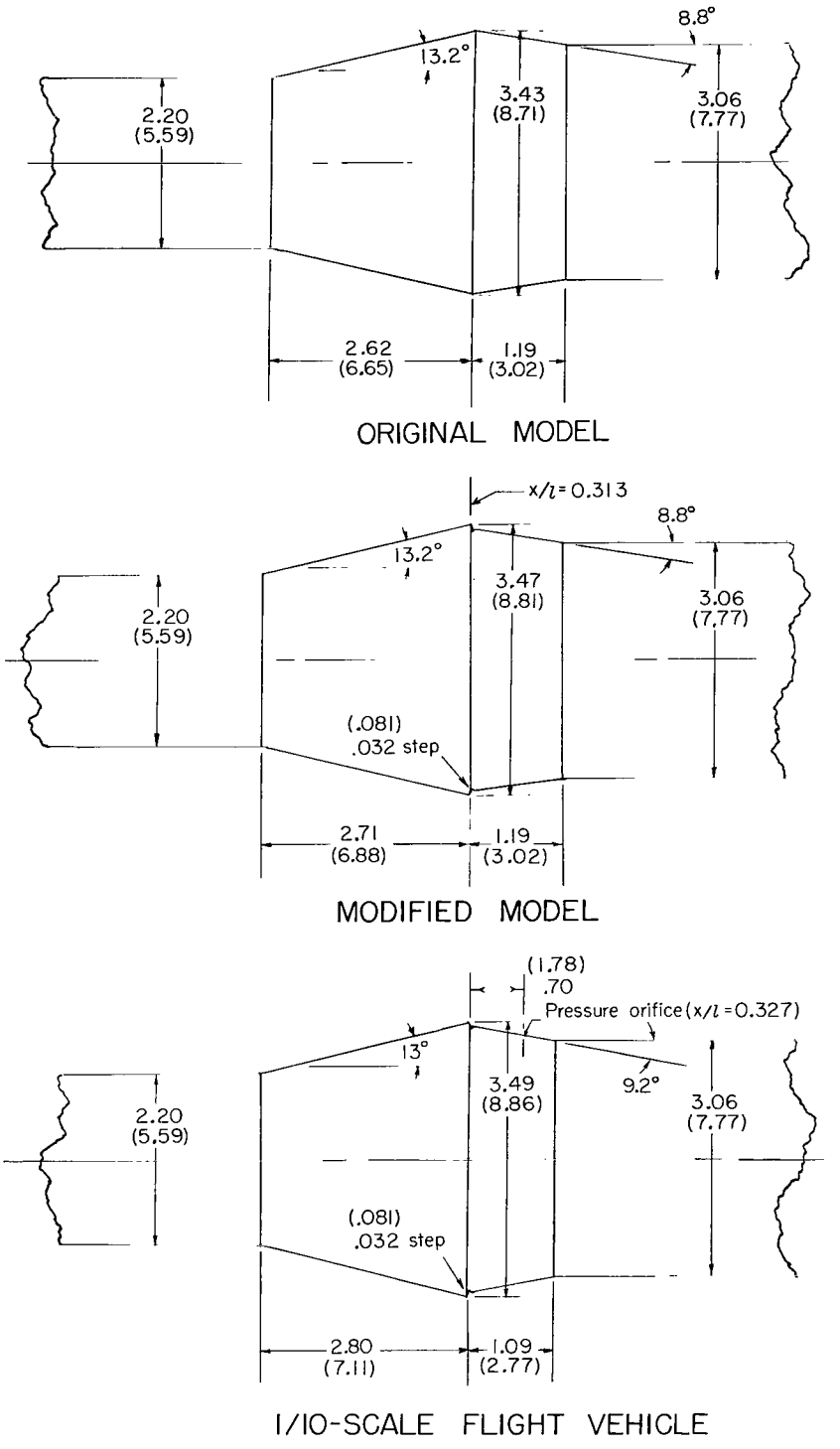

Figure 1.- Flare—reverse-flare details for original model, modified model, and 1/10-scale flight vehicle. Dimensions are given first in inches and parenthetically in centimeters.

(a) Ram vehicle on launcher. L-63-4919

Figure 2.- Photographs of flight vehicle.

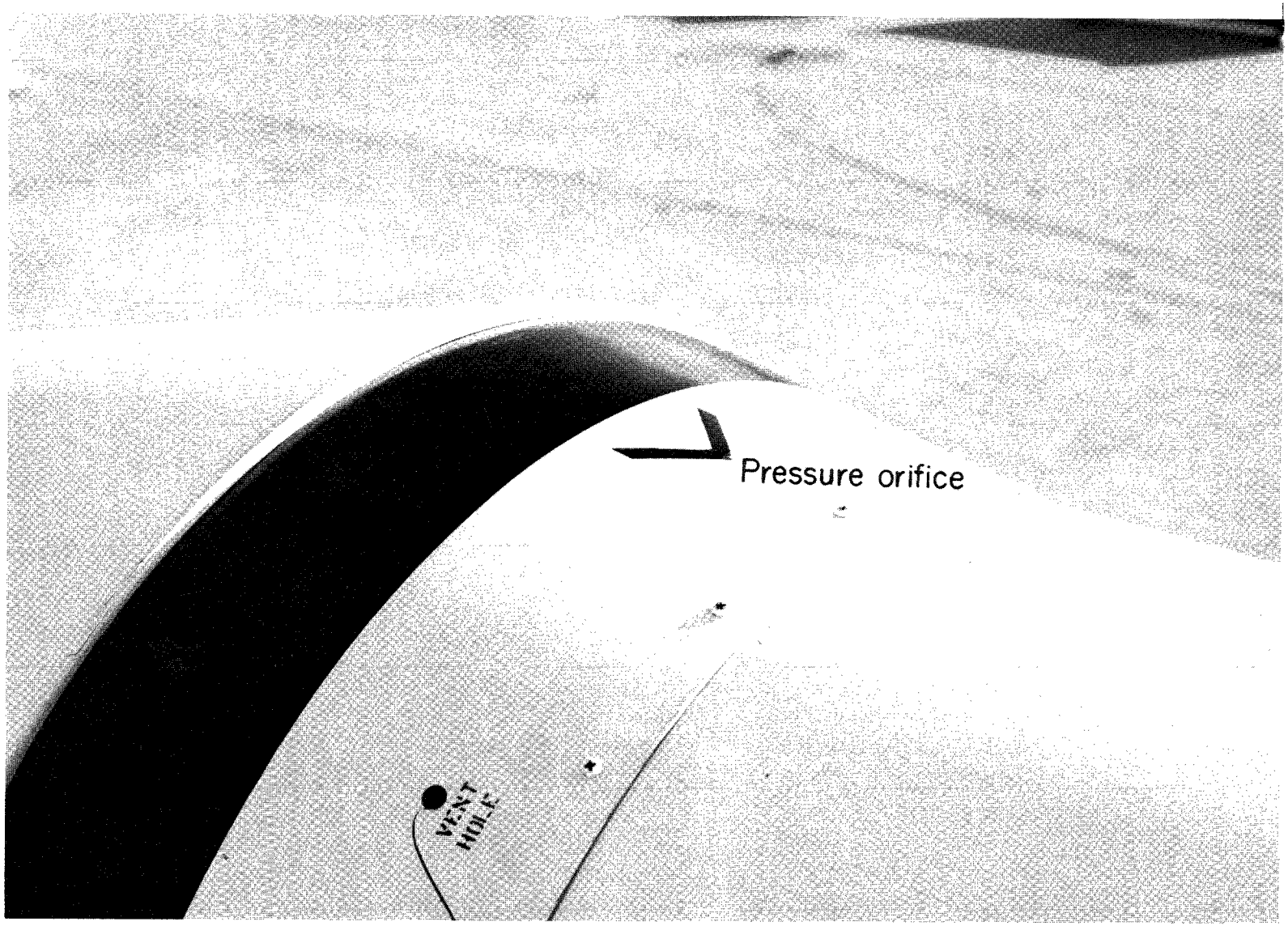

(b) Reverse-flare details.

L-64-2688.1

Figure 2.- Concluded.

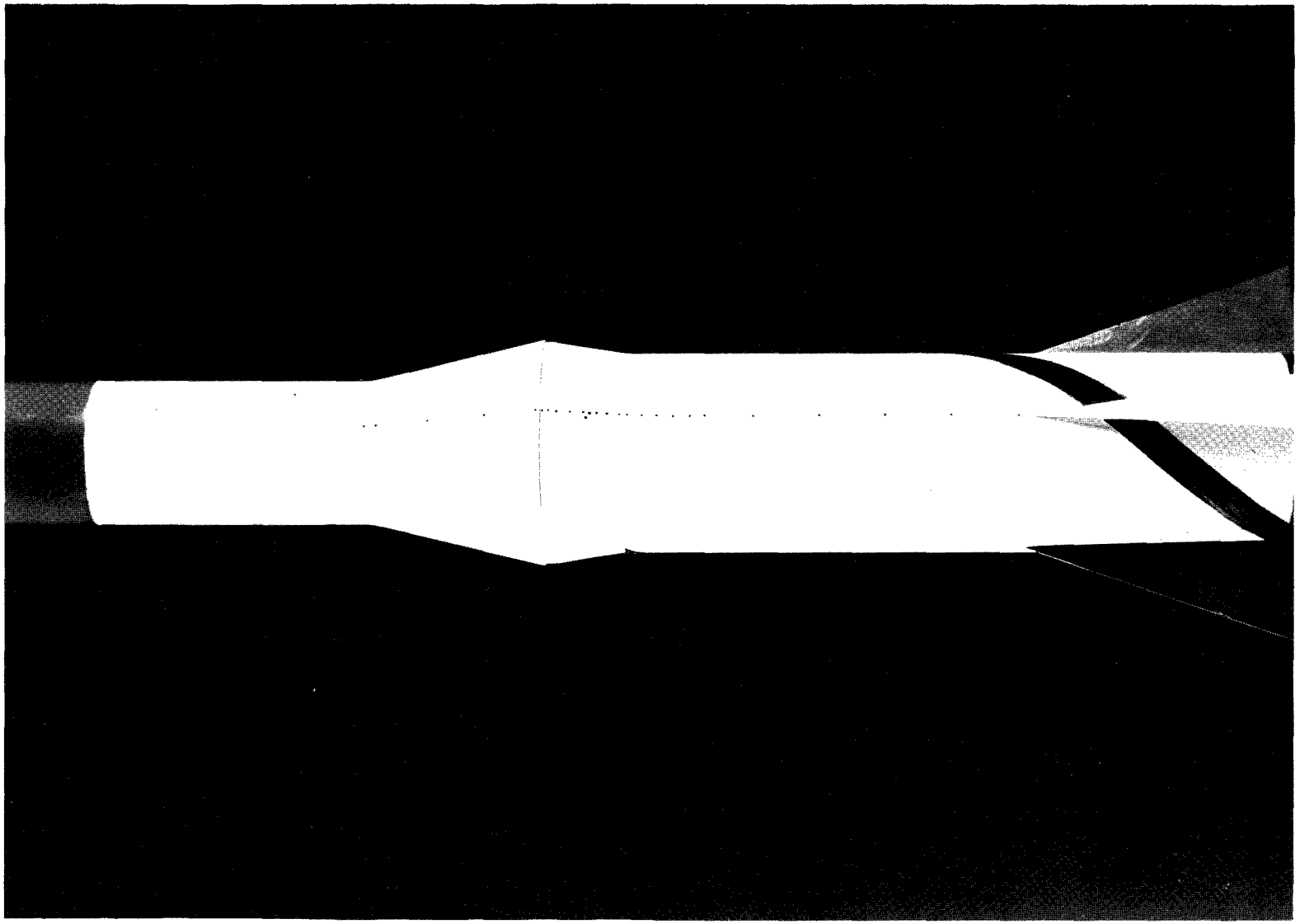

(a) Instrumented region. L-64-8436

Figure 3.- Photographs of wind-tunnel model.

L-64-8435

(b) Flare and step details.

Figure 3.- Concluded.

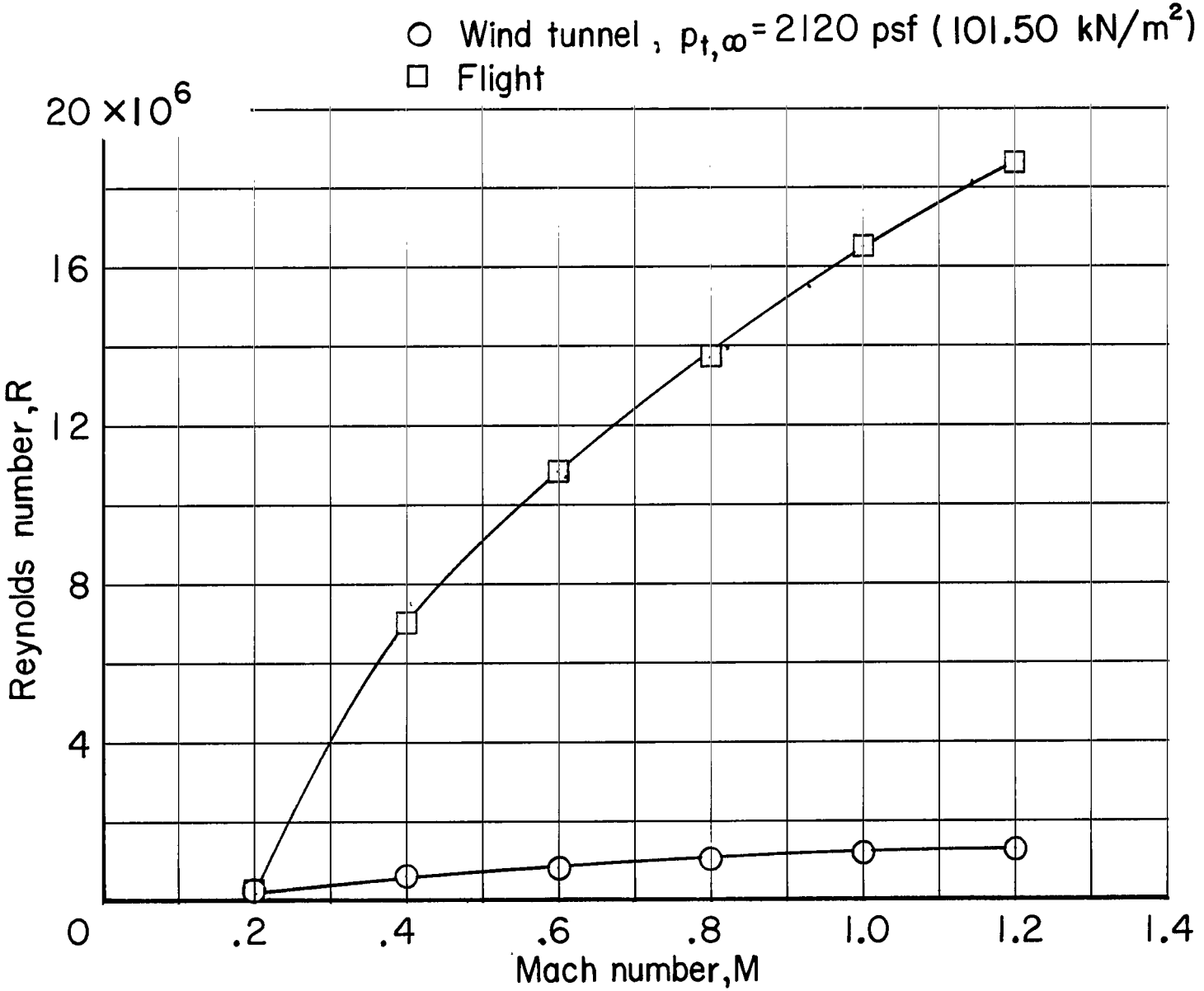

Figure 4.- Variation with Mach number of Reynolds number based on first-stage diameter for flight and wind-tunnel configurations.

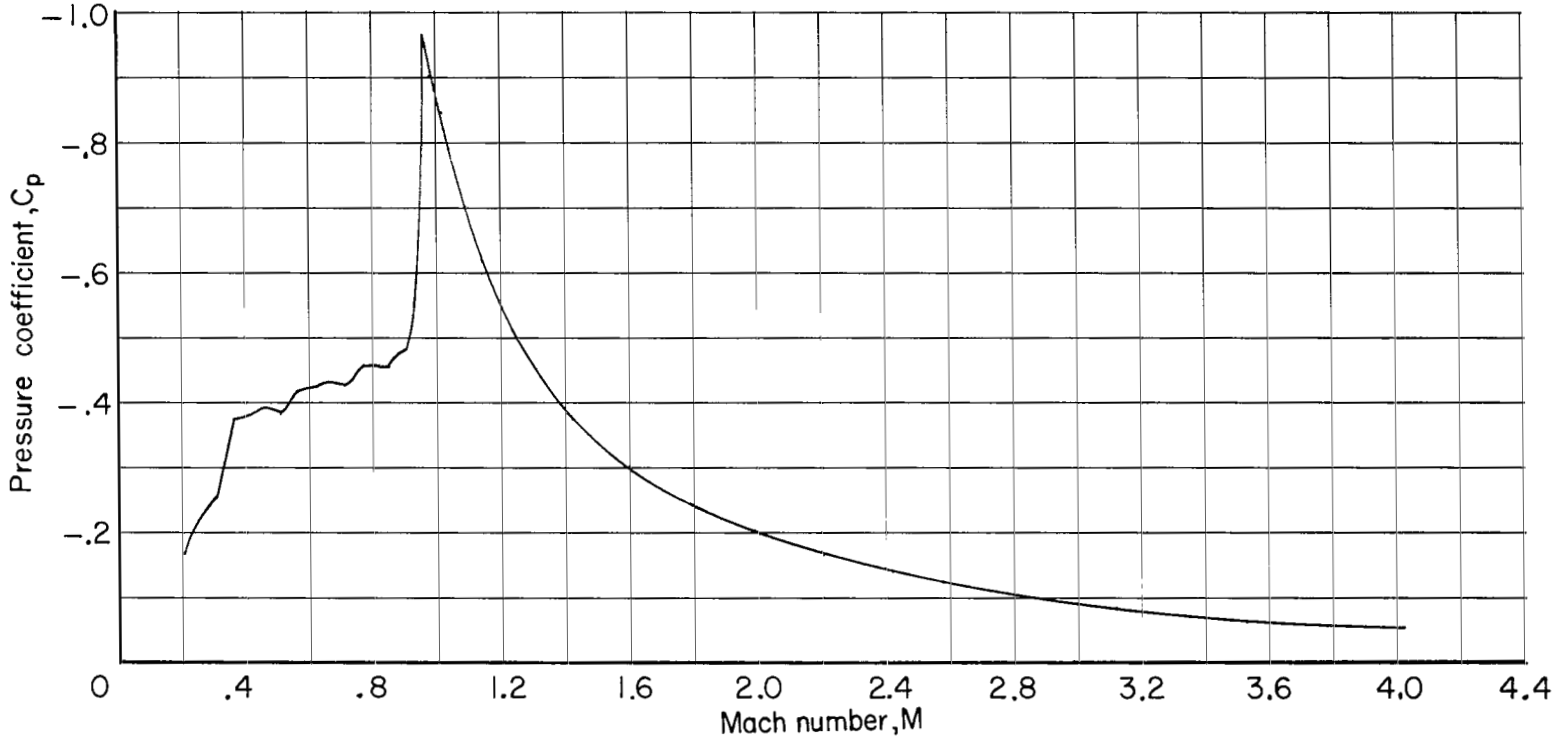

(a) Variation of pressure coefficient with Mach number.

Figure 5.- Flight pressure measurements. $\frac{x}{l} = 0.327$.

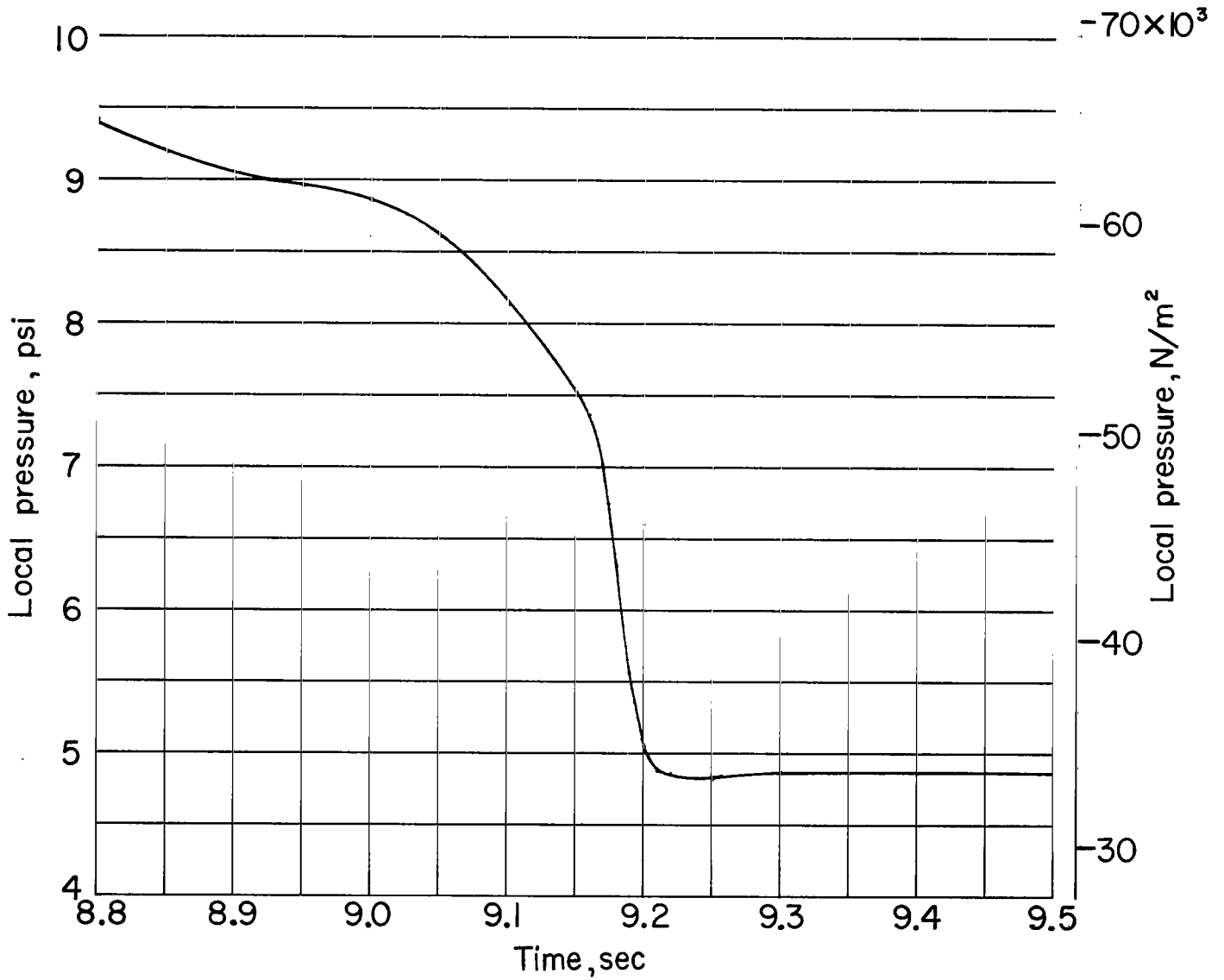

(b) Variation of local pressure with time.

Figure 5.- Concluded.

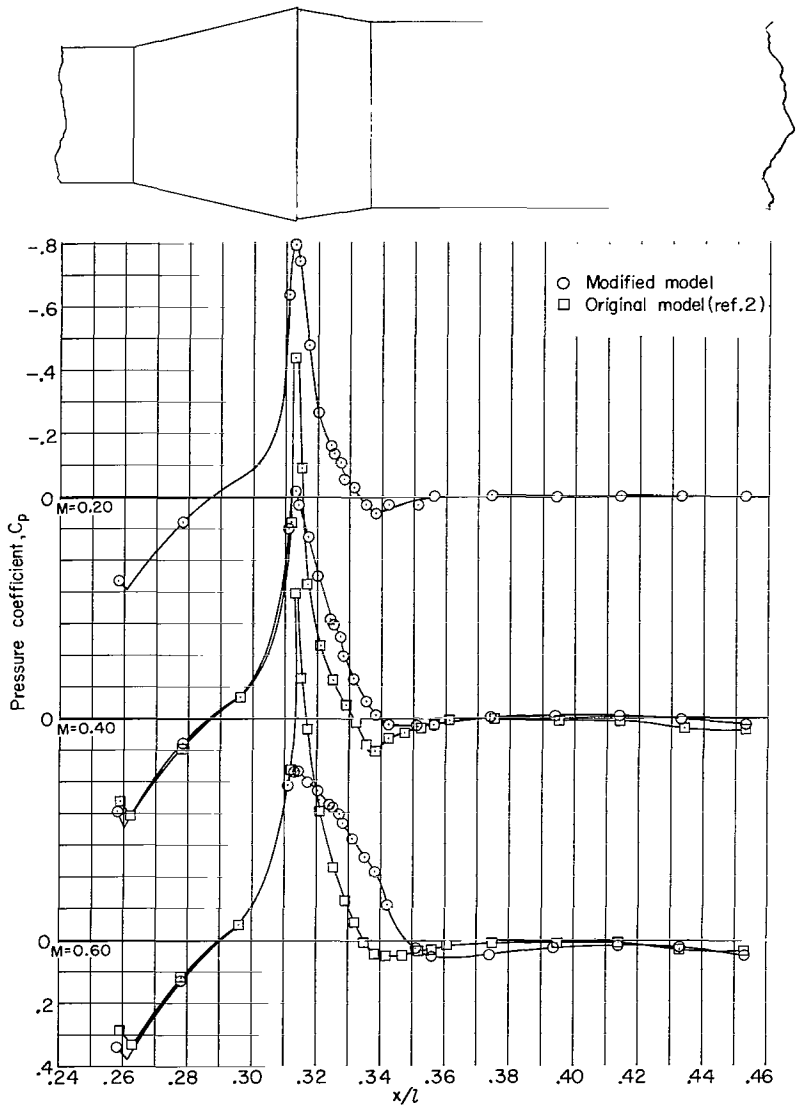

(a) M = 0.20, 0.40, and 0.60.

Figure 6.- Wind-tunnel measurements. $p_{t,\infty}$ = 2120 psf (101.51 kN/m^2).

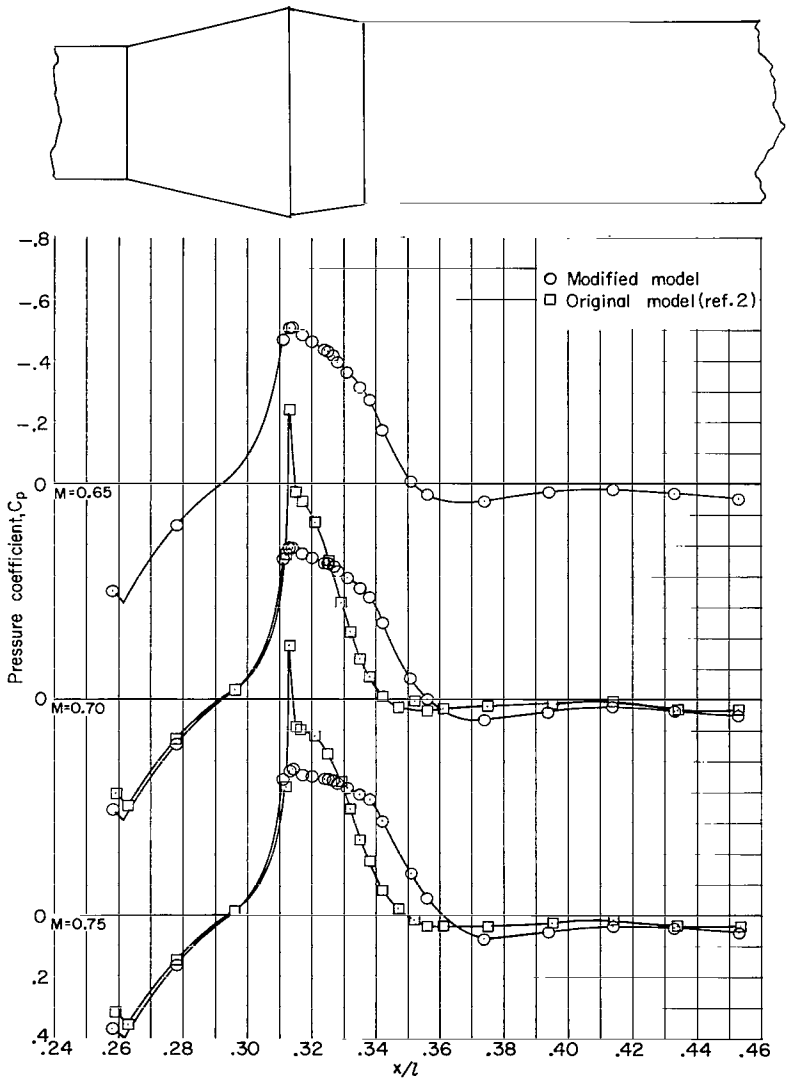

(b) M = 0.65, 0.70, and 0.75.

Figure 6.- Continued.

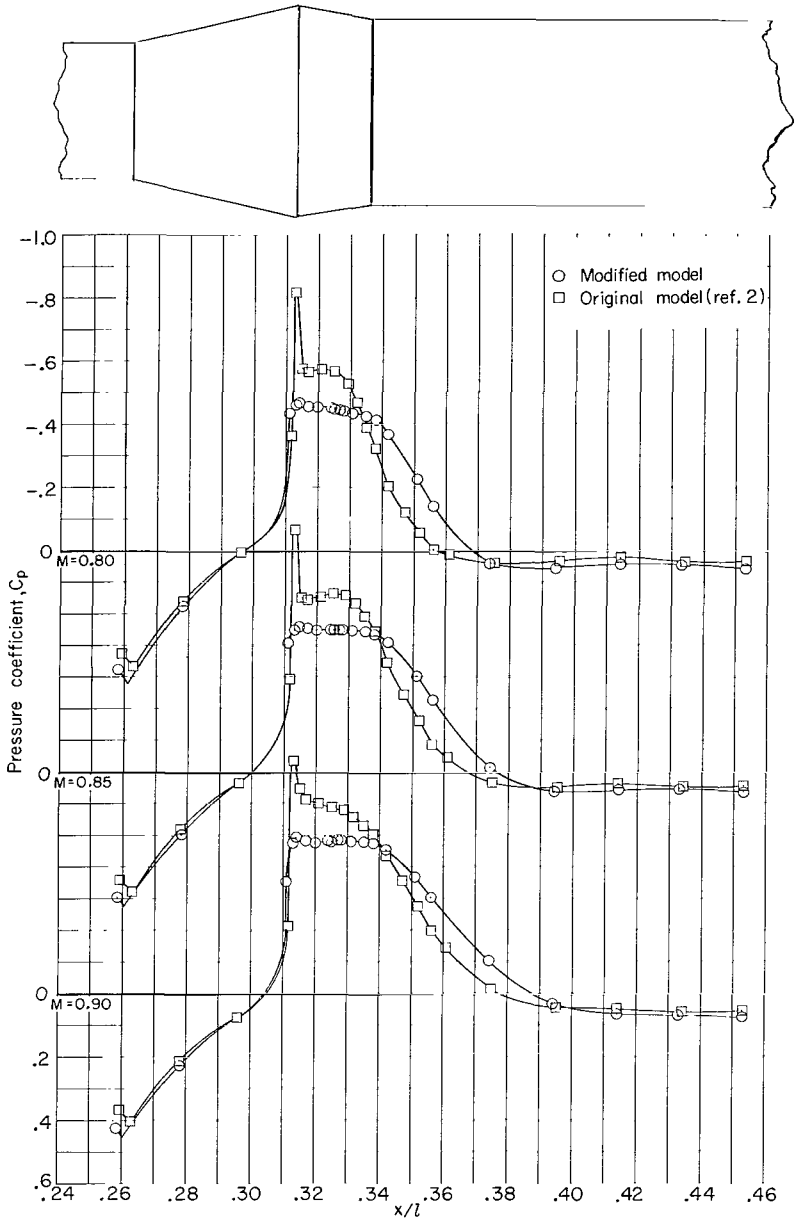

(c) M = 0.80, 0.85, and 0.90.

Figure 6.- Continued.

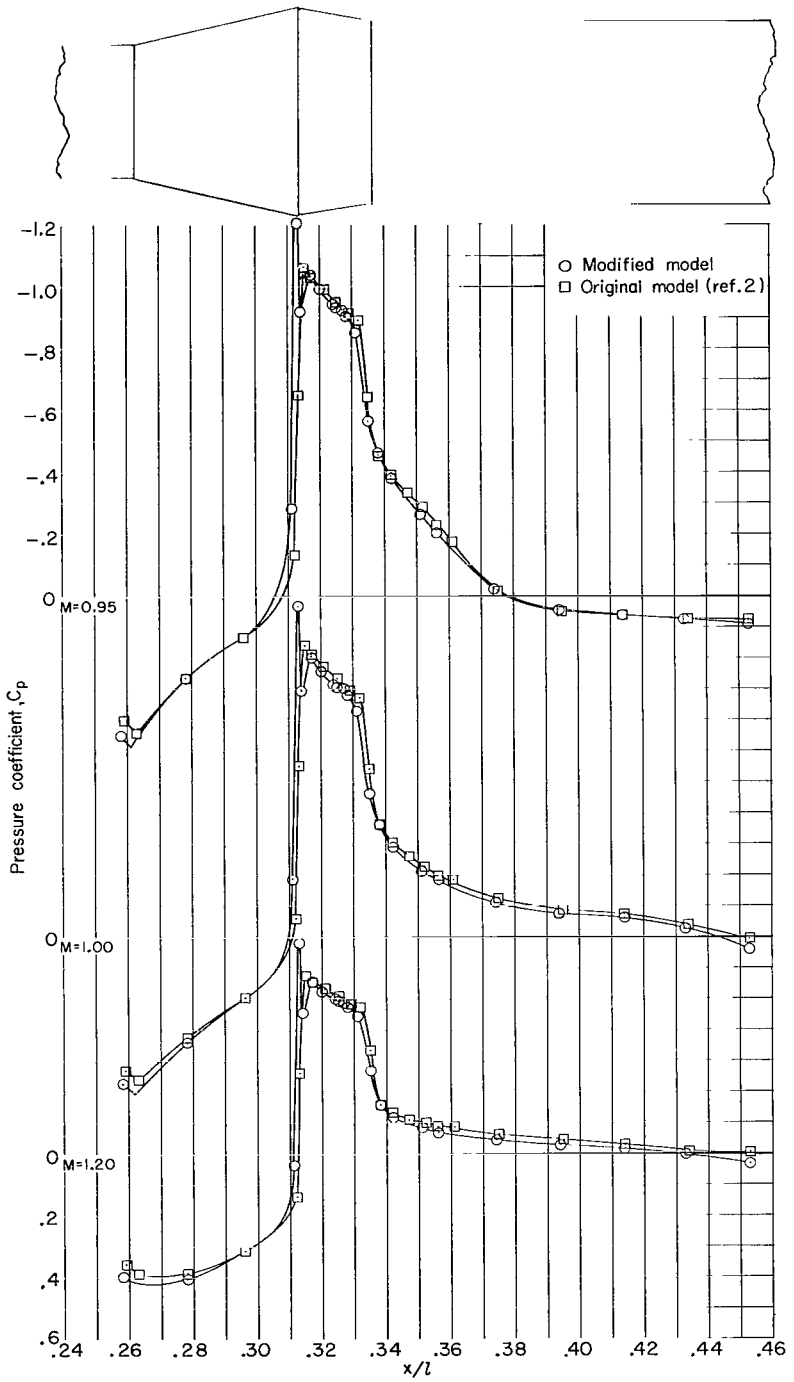

(d) M = 0.95, 1.00, and 1.20.

Figure 6.- Concluded.

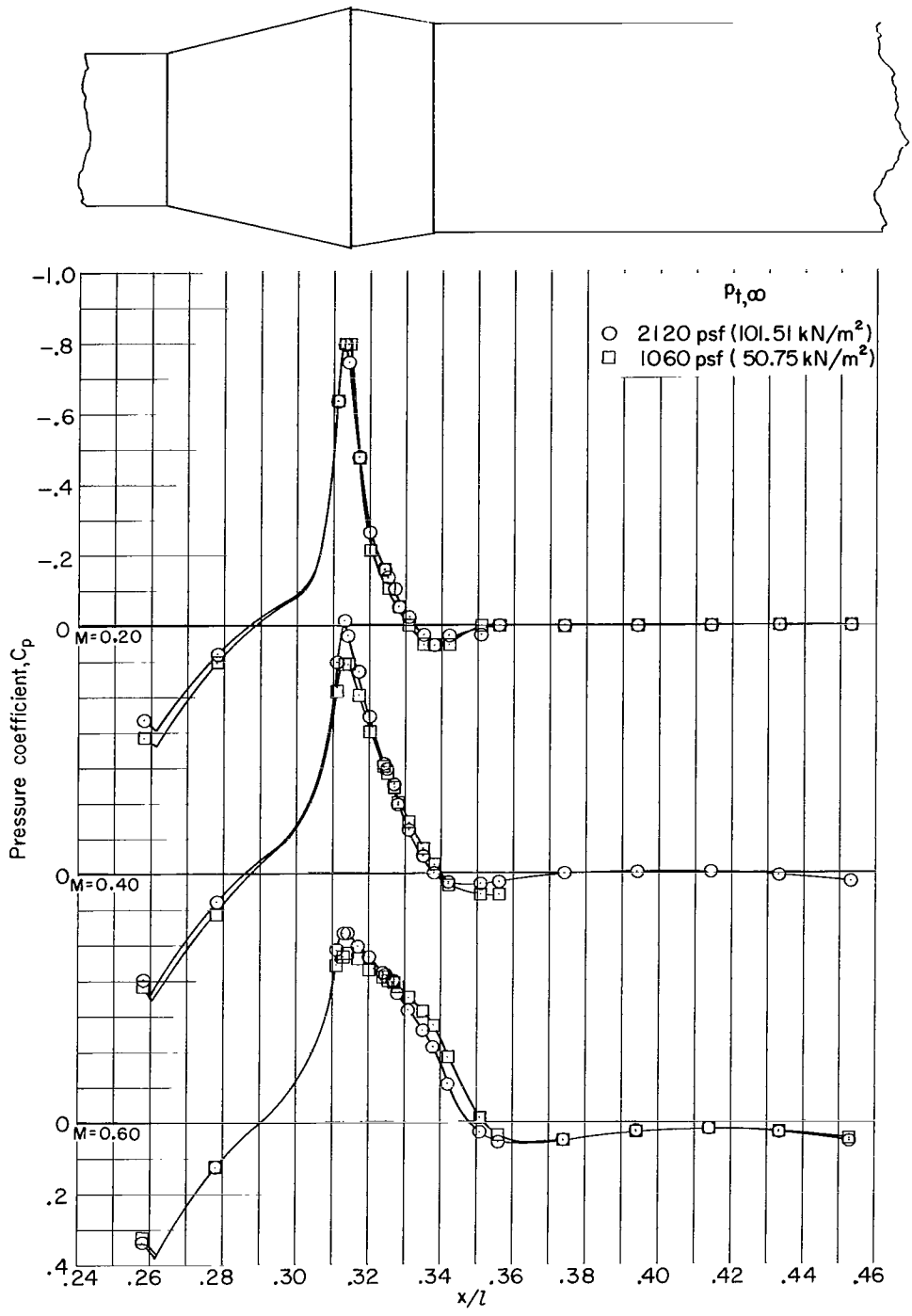

(a) M = 0.20, 0.40, and 0.60.

Figure 7.- Effect of tunnel stagnation pressure on pressure coefficients for modified model configurations.

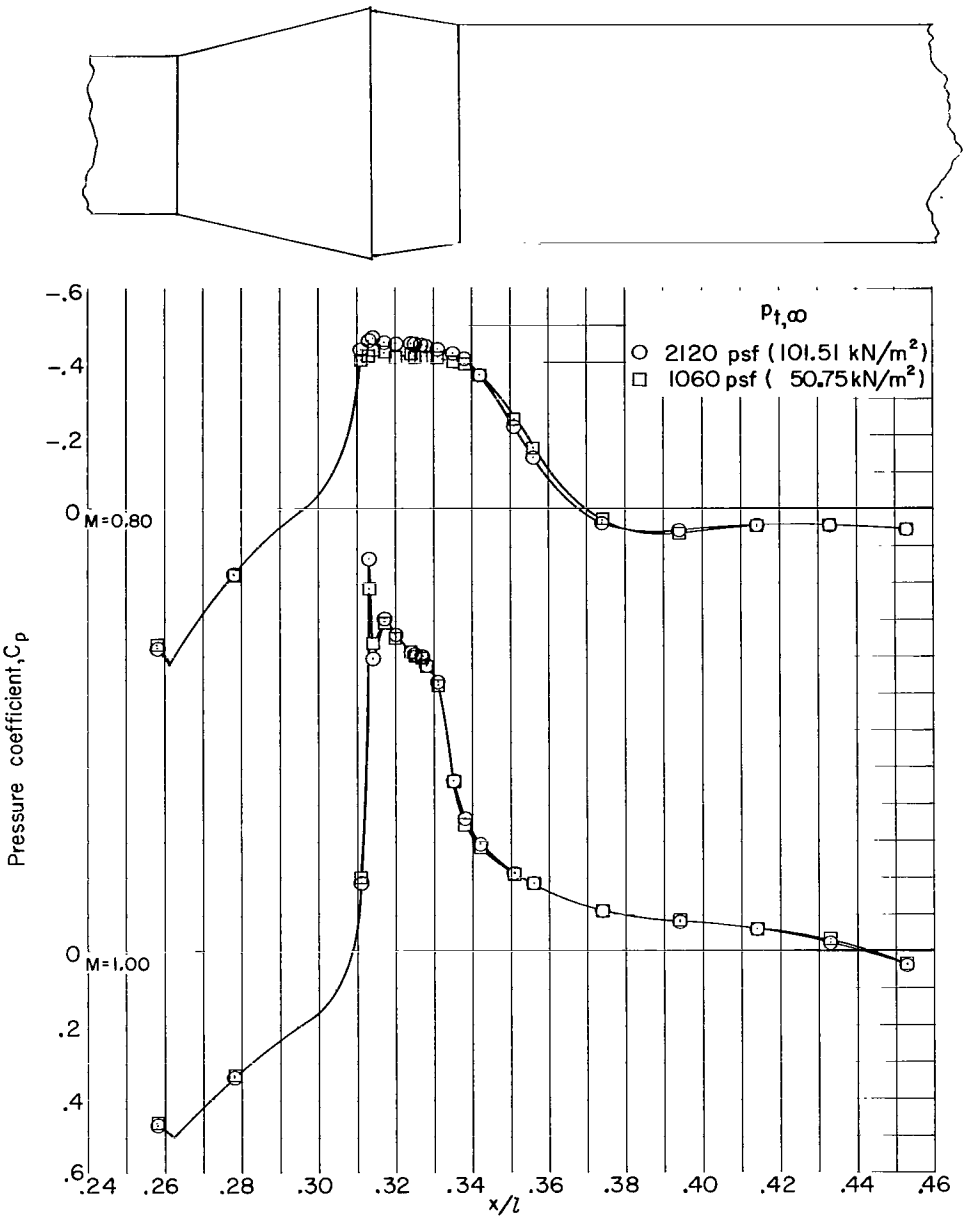

(b) M = 0.80 and 1.00.

Figure 7.- Concluded.

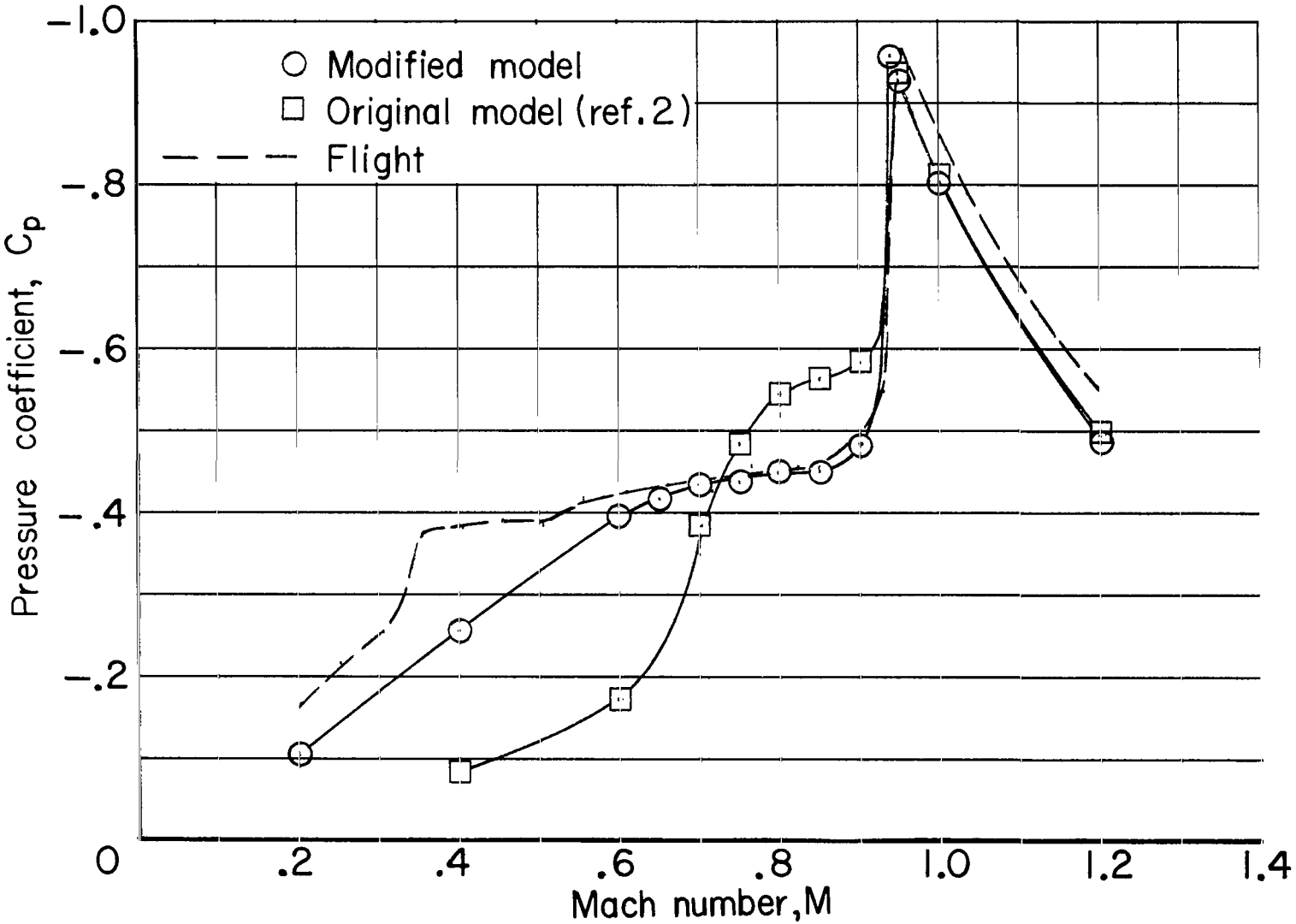

Figure 8.- Comparison of flight and wind-tunnel results. $\frac{x}{l} = 0.327$.

"The aeronautical and space activities of the United States shall be conducted so as to contribute . . . to the expansion of human knowledge of phenomena in the atmosphere and space. The Administration shall provide for the widest practicable and appropriate dissemination of information concerning its activities and the results thereof."

—NATIONAL AERONAUTICS AND SPACE ACT OF 1958

NASA SCIENTIFIC AND TECHNICAL PUBLICATIONS

TECHNICAL REPORTS: Scientific and technical information considered important, complete, and a lasting contribution to existing knowledge.

TECHNICAL NOTES: Information less broad in scope but nevertheless of importance as a contribution to existing knowledge.

TECHNICAL MEMORANDUMS: Information receiving limited distribution because of preliminary data, security classification, or other reasons.

CONTRACTOR REPORTS: Technical information generated in connection with a NASA contract or grant and released under NASA auspices.

TECHNICAL TRANSLATIONS: Information published in a foreign language considered to merit NASA distribution in English.

TECHNICAL REPRINTS: Information derived from NASA activities and initially published in the form of journal articles.

SPECIAL PUBLICATIONS: Information derived from or of value to NASA activities but not necessarily reporting the results of individual NASA-programmed scientific efforts. Publications include conference proceedings, monographs, data compilations, handbooks, sourcebooks, and special bibliographies.

Details on the availability of these publications may be obtained from:

SCIENTIFIC AND TECHNICAL INFORMATION DIVISION

NATIONAL AERONAUTICS AND SPACE ADMINISTRATION

Washington, D.C. 20546